PODOPLANIN-TARGETABLE MR/OPTIC DUAL-MODE NANOCOMPOSITES FOR GLIOBLASTOMA MULTIFORME IN MOUSE BRAIN CANCER

H. LEE[a,b,c], E. J. CHO[a], H. SON[a,h], H.O. KIM[d], Y. HONG[e], S. H. YANG[a,f],
S. J. YOON[g,i], J. H. LEE[g], J. K. SHIM[g], J. H. CHANG[g], S.G. KANG[g,],
Y. M. HUH[a,b,f,i,*]

[a]*Department of Radiology, College of Medicine, Yonsei University,
Seoul 120-752, Republic of Korea*
[b]*YUHS-KRIBB Medical Convergence Research Institute, College of Medicine,
Yonsei University, Seoul 120-752, Republic of Korea*
[c]*Graduate Program of Nanoscience and Technology, College of Medicine, Yonsei
University, Seoul 120-752, Republic of Korea*
[d]*Department of Biotechnology and Bioengineering, Kangwon National University,
Chuncheon, Gangwon-do 24341, Republic of Korea*
[e]*Department of Medical Devices, Korea Institute of Materials (KIMM), Daegu
42994, Republic of Korea*
[f]*National Core Research Center, Nanomedical Interdisciplinary Program, Yonsei
University, Seoul 120-749, Republic of Korea*
[g]*Department of Neurosurgery, Brain Tumor Center, Severance Hospital, College
of Medicine, Yonsei University, Seoul 120-752, Republic of Korea*
[h]*Severance Biomedical Science Institute, Seoul 120-749, Republic of Korea*
[i]*Department of Biochemistry and Molecular Biology, College of Medicine, Yonsei
University, Seoul 120-752, Republic of Korea*

It is very desirable to design dual-mode nanocomposites for diagnostic applications via flexible strategies. Herein, we proposed to synthesize one type of multifunctional magnetic resonance (MR)/optic nanocomposites based on manganese ferrite magnetic nanoparticles (MFNPs) modified by fluorescent podoplanin (PDPN) antibodies. MFNPs were synthesized using a thermal decomposition method and were modified by the fluorescent PDPN antibodies on their surfaces. The fluorescent PDPN antibody-conjugated MFNPs enabled strong MR imaging and fluorescence imaging due to the antibodies that targeted brain tumors. These results demonstrate that MR/optic nanocomposites have potential as precision diagnostic systems for brain cancer.

1. Introduction

Medical imaging technologies, such as magnetic resonance imaging (MRI), X-ray computed tomography (CT), ultrasound imaging, and optical imaging, have been widely used for disease diagnosis.[1-5] However, it is difficult for any single imaging modality to provide sufficient information for a precise diagnosis. A promising strategy is to develop multimodal contrast agents for different imaging modalities, such as MRI/CT, CT/fluorescence imaging, and MRI/ultrasound imaging, which can combine their individual advantages in disease diagnosis. [6-8] Specifically, MRI has emerged as a key tool in the diagnosis of cancer, since it has advantages over noninvasive anatomical imaging due to its high resolution, high contrast, and ability to provide three-

---

* Corresponding author: ymhuh@yuhs.ac

dimensional information in real time, much more so than nuclear medicine (positron electron tomography and single-photon emission computed tomography).[9,10] In addition, molecular MRI is able to detect simultaneously the metabolism of cells and tissues, physiological and structural information, and biological processes occurring in deep tissues.[11-14] In particular, the use of near-infrared (NIR) light (700 ~ 1,000 nm) for optical imaging can penetrate several centimeters into tissue, because hemoglobin and water, the primary absorbers of visible and infrared light, experience their lowest absorptions in the NIR region. Thus, NIR imaging offers a potentially non-invasive and real-time characterization of diseased tissues using optical imaging probes including quantum dots and fluorescent-dye-doped nanoparticles.[15-19]

Glioblastoma multiforme is a lethal intracranial cancer, which exhibits a relentless malignant progression that is highly resistant to conventional combination therapies such as traditional radiation and chemotherapy agents.[20] Therefore, the early detection of glioblastoma is very crucial for effective treatment. Traditionally, as MRI plays a major role in the imaging of neovascularization in the tumor's micro-environment, it is crucial in predicting the metastasis of the cancer.[21] However, the weak point of MRI is sensitivity; the use of optical imaging enables us to increase the sensitivity and compensate for the disadvantages of MRI.[22] In particular, it can increase the contrast and sensitivity for new blood vessels, which can cause great synergy.[23]

Herein, we proposed to synthesize one magnetic resonance (MR)/optic dual-mode nanocomposites based on manganese ferrite magnetic nanoparticles (MFNPs) modified with fluorescent podoplanin antibodies. The fluorescent podoplanin antibody-conjugated MFNPs enabled strong MRI and fluorescence imaging due to the antibodies targeted to the brain tumor. These results demonstrate that MR/optic nanocomposites have potential as precision diagnostic systems for brain cancer (Scheme 1).
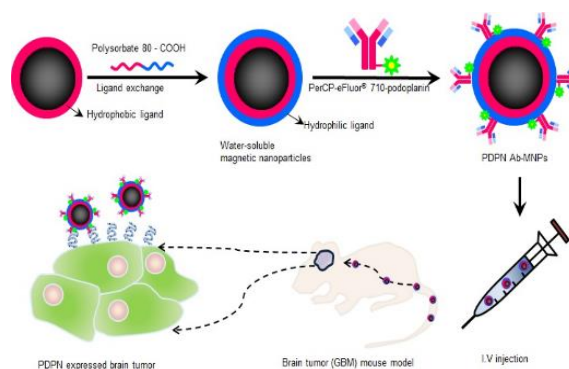
Scheme 1. Schematic illustration of PDPN-targetable opto-magnetic nanoprobes for molecular imaging of brain cancer. GBM, glioblastoma multiform

2. Experiment details

2.1. Materials

Polysorbate 80, ethylenediamine, 1,4-dioxane (99.8%), 4-dimethylaminopyridine, triethylamine, and succinic anhydride (SA) were purchased from Sigma Aldrich Chemical Co. Phosphate buffered saline (PBS: 10 mM, pH 7.4) and Dulbecco's modified Eagle's medium (DMEM) were purchased from Corning Incorporated, 1x B27 supplement was purchased from Invitrogen, and basic fibroblast growth factor (bFGF: 20 ng/ml) and epidermal growth factor (EGF: 20 ng/ml) were purchased from Sigma. Fetal bovine serum (FBS) and antibiotic-antimycotic solution were purchased from Gibco. GSC11 cell lines (American Type Culture Collection) were grown in medium containing 10% fetal bovine serum and 1% antibiotic-antimycotic at 37 °C in a humidified 5% CO_2 atmosphere. Ultrapure deionized water was used for all of the syntheses.

2.2. Synthesis of magnetic nanoparticles
To synthesize monodispersed magnetic nanoparticles (MNPs), 2 mmol of iron (III)

acetylacetonate, 1 mmol of manganese(II) acetylacetonate, 10 mmol of 1,2-hexadecanediol, 6 mmol of dodecanoic acid, and 6 mmol of dodecylamine were dissolved in 20 mL of benzyl ether under an ambient nitrogen atmosphere. The mixture was then pre-heated to 200 °C for 2 hours and refluxed at 300 °C for 30 minutes. After the reactants were cooled to room temperature, the products were purified with an excess of pure ethanol. Approximately 11 nm of MFNPs were synthesized using the seed-mediated growth method.[24,25,26]

2.3. Modification of polysorbate 80

To prepare charged MNPs, the hydroxyl groups of the NPs were modified with carboxyl groups. For the preparation of carboxylated polysorbate 80 (anionic polysorbate, AP) using SA, first, 5 mmol NP and 20 mmol SA were dissolved in a flask containing 100 ml of 1,4-dioxane, and the reactant solution was stirred for 1 h. Subsequently, 20 mmol dimethylaminopyridine and triethylamine were added to the reactor at room temperature. After further reaction for 24 h, the unwanted solvent was rapidly eliminated using a rotary evaporator. The obtained transparent gel-type product was then dissolved in 10 ml of deionized water and dialyzed against an excess aqueous phase for at least seven days. The purified product was freeze-dried and stored under vacuum for later use. The characteristic bands of modified polysorbate 80 were confirmed by Fourier-transform infrared spectroscopy.

2.4. Preparation of PDPN-targetable opto-magnetic nanoprobes

Three types of carboxylated MFNPs were prepared by the nanoemulsion method. The MFNPs (30 mg) were dissolved in 4 ml of hexane (as the organic phase), and the organic phase was then mixed with 20 ml of deionized water (as the aqueous phase) containing 100 mg carboxylated polysorbate 80. After mutual saturation of the organic and aqueous phases, the emulsion was ultra-sonicated in an ice-cooled bath for 15 min at 190 W. Next, the organic solvent was evaporated overnight at room temperature, and the products were purified by centrifugal filtration (Centriprep YM-3, 3,000 Da, Amicon) with two cycles at 3,000 rpm for 1 h. PerCP-eFluor® 710-podoplanin-coated MFNPs were fabricated by 1-ethyl-3-(-3-dimethylaminopropyl) carbodiimide hydrochloride (EDC)-N-hydroxysuccinimide (NHS) chemistry. First, the pH of the aminated MFNP solution was adjusted to a neutral condition by the addition of 0.1 N HCl solution. Then, PerCP-eFluor® 710-podoplanin was dissolved in the 40 ml of de-ionized water followed by the addition of EDC and sulfo-NHS.

2.5. Biocompatiblility test for PDPN-targetable opto-magnetic nanocomposites

The cytotoxic effects of PDPN-targetable opto-magnetic nanocomposites in GSC11 were evaluated by 3-(4,5-dimethylthiazol-2-yl)-2,5-diphenyltetrazolium bromide (MTT) assay. GSC11 cells were maintained in DMEM with 10% FBS and 1% antibiotics at 37 °C in a humidified atmosphere with 5% CO_2. GSC11 cells (1.0×10^4 cells/well) were seeded into a 96-well plate at 37 °C overnight, and the cells were then incubated with various concentrations of PDPN-targetable opto-magnetic nanocomposites for 4 h. The cells were washed with 100 μl of PBS (pH 7.4, 1 mM), and 100 μl of phenol red-free DMEM were added. Subsequently, the cells were treated with MTT assay solution according to the manufacturer's instructions. Cell viability was evaluated using a microplate reader (Synergy H4 hybrid reader, BioTek) at an absorbance wavelength of 575 nm (reference wavelength of 650 nm).

2.6. Prussian blue staining

GSC11 cells (1.0×10^6 cells/well) were seeded into 6-well plates and incubated at 37 °C. Various prepared concentrations of PDPN opto-magnetic nanocomposites were mixed with DMEM, and these mixtures were added to the cells. After incubation for 4 h at 37 °C, the cells were washed with PBS and fixed with 4% paraformaldehyde. The working solution was prepared by mixing 10% potassium ferrocyanide and 20% HCl in equal amounts. The working solution was added to the cells and incubated for 30 min at room temperature. The cells were then washed with PBS and stained with nuclear fast red solution for 30 min at room temperature. The cells were observed using an optical system microscope (Olympus BX51, Japan).

2.7. Animal model and experimental procedure

All animal experiments were conducted with the approval of the Association for Assessment and Accreditation of Laboratory Animal Care International. Female BALB/C-Slc nude mice at 7-8 weeks of age were anesthetized by intraperitoneal injection of a Zoletil/Rompun mixture and injected with 200 ml containing 1.0×10^7 GSC11 cells suspended in saline into the brain. After cancer cell implantation, MRI was performed between two and three weeks. After MRI, organ MRI was also performed. In addition, the extracted tumor tissues from the tumor-bearing brains treated with opto-magnetic nanoparticles were sectioned and stained using Prussian blue. All stained tissue sections were analyzed using a virtual microscope (Olympus BX51, Japan) and OlyVIA software (Olympus).

2.8. Magnetic resonance imaging

We performed solution and in vitro MRI experiments with a 3T clinical MRI instrument with a micro-47 surface coil (Intera, Philips Medical Systems, Best, The Netherlands). The R2 (T2 relaxation rate, $1/T2$, $s-1$) was measured using the Carr-Purcell-Meiboom-Gill sequence at room temperature with the following parameters: TR = 10 s, 32 echoes with 12 ms even echo space, number of acquisitions = 1, point resolution of 156×156 m, and section thickness of 0.6 mm. Additionally, in vivo MRI experiments were performed with a 3T Siemens clinical MRI instrument using a human wrist coil with a T2 TSE sequence (TR: 4,000 ms, TE: 114 ms, slice thickness: 1.0 mm, FOV read: 180 mm).

2.9. Optical imaging

GSC11 brain tumor-bearing mice were imaged by positioning each mouse on an animal plate, heated to 37 °C, in the IVIS spectrum system (Caliper Life Science, Hopkinton, MA, USA) per the manufacturer's instructions. Excitation and emission spots were raster-scanned over the selected region of interest (ROI) to generate emission wavelength scans; the wavelengths of fluorescence were 488 nm and 520 nm, respectively, for the ex vivo samples. All data, including whole body and two-dimensional slice images, were calculated using the ROI function of the Analysis Workstation software.

3. Results and discussion

3.1. Cell viability testing of PDPN opto-magnetic nanocomposites

The MTT assay was performed, in which yellow tetrazolium salt is reduced to purple formazan crystals in metabolically active cells. The relative percentage of cell viability was determined as the ratio of formazan intensity in viable cells that were treated with PDPN opto-magnetic nanoprobes to the intensity in the cells. As shown in Fig. 1, the in vitro cytotoxicity measured by MTT assay showed that the viability of GSC11 cells was about 80% at a concentration of 3.98 μg Fe + Mn/ml.
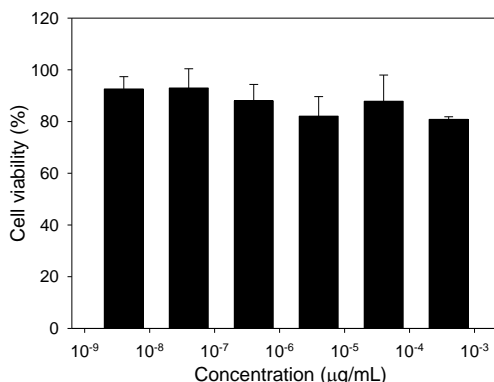

Fig. 1. In vitro cytotoxicity test for PDPN opto-magnetic nanocomposites for in vivo dual image analysis.

3.2. In vivo dual image analysis

In Fig. 2, MR signal enhancement was identified after injection with PDPN-based opto-magnetic nanoparticles. Initially, the center of the tumor darkened instantly, and enhanced MRI signal intensity at the surrounding vessels was simultaneously observed. In T2 TSE MR images, clear anatomic details were observed, and there were no artifacts due to a difference in susceptibility. The anatomic details were also clear in the optical images observed via fluorescence as time elapsed.
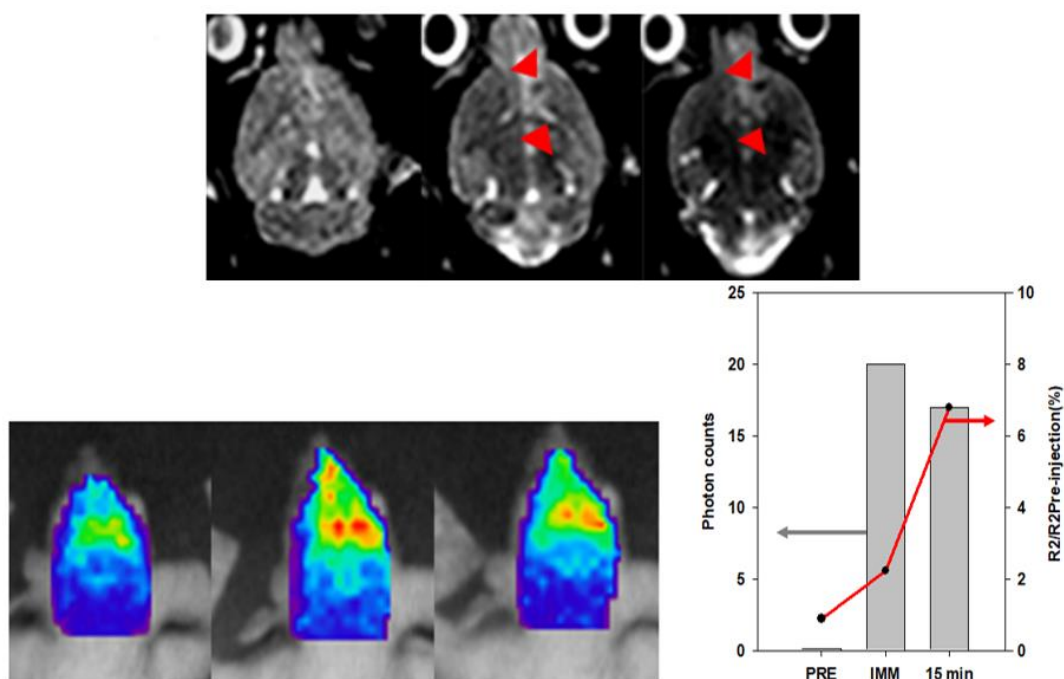

Fig. 2. In vivo MR and optical imaging using PDPN opto-magnetic nanocomposites:
(A) MR images, (B) optical images, and (C) quantitative graphs of A and B.

3.3. Histological analysis

In Fig. 3(A), we confirmed the tumor's morphology using hematoxylin and eosin staining. This demonstrated the property of the tumor cells, which had more and larger nuclei. Therefore, we noticed that each of the cancer cells could be well identified through the hematoxylin (nuclei: blue) and eosin Y (cytoplasm: pink) staining. In Fig. 3(B), the iron contents (black arrows) of the accumulated opto-magnetic nanoprobes in the tumors were observed by Prussian blue staining. In Fig. 3(C), the podoplanin-targeted fluorescence in the tumor was observed by confocal microscope. Consequently, we confirmed that our developed opto-magnetic nanoprobes for dual imaging have adequate capability for the targeted imaging of brain cancer overexpressing brain PDPN.
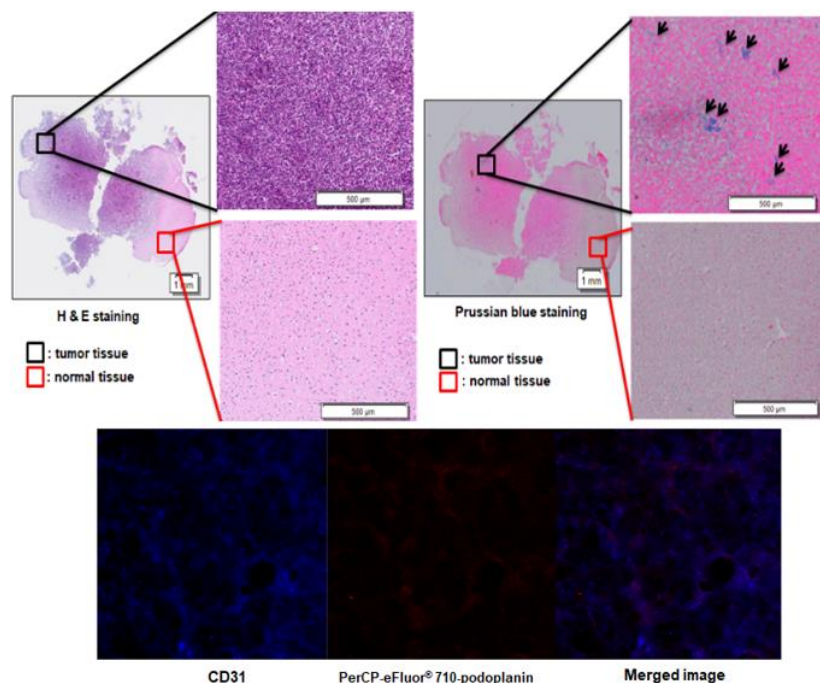
Fig. 3. Histological analysis for PDPN opto-magnetic nanocomposites.

4. Conclusion

The potential application of a dual imaging probe for MR and optical imaging in glioblastoma multiform diagnosis using a GSC11 brain cancer model was investigated based on a mouse brain cancer model. Our results suggested that the dual probe for MR and optical probe imaging was able to improve the diagnostic application for glioma. Such findings might have a great impact on clinical studies for the early detection of brain cancer. In addition, this method makes it possible to use a variety of imaging devices, thus ameliorating the disadvantages of each imaging device. Further investigations are warranted to evaluate the potential of this technique in clinical settings.

Abbreviations

MRI: magnetic resonance imaging; MFNPs: manganese ferrite magnetic nanoparticles; PDPN: podoplanin; GBM: glioblastoma multiforme.

Acknowledgements

References

[1] J. H. Lee, Y. M. Huh, Y. W. Jun, J. W. Seo, J. T. Jang, H. T. Song, S. Kim, E. ZJ. Cho, H. G. Yoon, J. S. Suh, J. Cheon, Nature Med. **13**, 95 (2007).
[2] R. Weissleder, M. J. Pittet, Nature **452**, 580 (2008).

[3] M. Rudin, R. Weissleder, Nature Rev Drug Discovery **2**, 123 (2003).

[4] M. Desai, A. L. Slusarczyk, A. Chapin, M. Barch, A. Jasanoff, Nature Comn. **7**, 13607 (2016).

[5] M. A. Stammes, S. L. Bugby, T. Porta, K. Pierzchalski, T. Devling, C. Otto, J. Dijkstra, A. L. Vahrmeijer, L. F. de Geus-Oei, J. S. D. Mieog, Br. J. Surg. **105**(2), 69 (2018).

[6] D. Calle, P. Ballesteros, S. Cerdán, Methods Mol. Biol. **1718**, 441 (2018).

[7] W. Cao, X. Lu, Z. Cheng, Curr. Pharm. Des. **21**(14), 1908 (2015).

[8] J. C. Stendahl, A. J. Sinusas, J. Nucl. Med. **56**(10), 1469 (2015).

[9] F. Abolaban, F. Djouder, Digest J. of Nanomaterials and Biostructures. **15**(3), 649 (2020)

[10] T. Lee, L. X. Cai, V. S. Lelyveld, A. Hai, A. Jasanoff, Science **2**(344), 533 (2014).

[11] H. Lee, S. H. Yang, D. Heo, H. Son, S. Haam, J. S. Suh, J. Yang, Y. M. Huh, J. Nanosci. Nanotechnol. **16**(1), 196 (2016).

[12] L. J. Grimm, K. S. Johnson, P. K. Marcom, J. A. Baker, M. S. Soo, Radiology **274**(2), 352 (2015).

[13] M. Haris, S. K. Yadav, A. Rizwan, A. Singh, E. Wang, H. Hariharan, R. Reddy, F. M. Marincola, J. Transl. Med. **23**(13), 313 (2015).

[14] D. M. Wilson, J. Kurhanewicz, J. Nucl. Med. **55**(10), 1567 (2014).

[15] M. Filippi, J. Martinelli, G. Mulas, M. Ferraretto, E. Teirlinck, M. Botta, L. Tei, E. Terreno, Chem. Commun. **50**(26), 3453 (2014).

[16] L. Leng, Y. Wang, N. He, D. Wang, Q. Zhao, G. Feng, W. Su, Y. Xu, Z. Han, D. Kong, Z. Cheng, R. Xiang, Z. Li, Biomaterials **35**(19), 5162 (2014).

[17] Y. Li, Y. Du, X. Liu, Q. Zhang, L. Jing, X. Liang, C. Chi, Z. Dai, J. Tian, Mol. Imaging **14**, 356 (2015).

[18] A. L. Antaris, H. Chen, K. Cheng, Y. Sun, G. Hong, C. Qu, S. Diao, Z. Deng, X. Hu, B. Zhang, X. Zhang, O. K. Yaghi, Z. R. Alamparambil, X. Hong, Z. Cheng, D. Dai, Nat. Mater. **15**(2), 235 (2016).

[19] R. S. Agnes, A. M. Broome, J. Wang, A. Verma, K. Lavik, J. P. Basilion, Mol. Cancer Ther. **11**(10), 2202 (2012).

[20] M. Satpathy, R. Zielinski, I. Lyakhov, L. Yang, Methods Mol. Biol. **1219**, 171 (2015).

[21] R. Li, X. Chen, Y. You, X. Wang, Y. Liu, Q. Hu, W. Yan, Oncotarget. **6**(31), 30968 (2015).

[22] L. B. Nilsen, A. Fangberget, O. M. Geier, O. Engebraaten, E. Borgen, D. R. Olsen, T. Seierstad, J. Magn. Reson. Imaging **40**(6), 1382 (2014).

[23] Y. Zhang, B. Zhang, F. Liu, J. Luo, J. Bai, Int. J. Nanomedicine **9**, 33 (2014).

[24] J. Zhou, Y. Sun, X. Du, L. Xiong, H. Hu, F. Li, Biomaterials **31**(12), 3287 (2010).

[25] S. Sun, H. Zeng, J. Am. Chem. Soc. **124**, 8204 (2002).

[26] L.K. Chuan, B. H. Guan, Y. Yusef, A.A. Zainuddin, N. Auni, Digest J of Nanomaterials and Biostructures **14**(1), 1 (2019).